The DRPM Strikes Back: More Flexibility for a Bayesian Spatio-Temporal Clustering Model

Author: FEDERICO ANGELO MOR

Advisor: PROF. ALESSANDRA GUGLIELMI

Co-advisor: ALESSANDRO CARMINATI

Academic year: 2023-2024

1. Introduction

Clustering is a fundamental technique of unsupervised learning where a set of data points has to be divided into homogeneous groups of units which exhibit a similar behaviour. It has long been a powerful tool for identifying structures and patterns within data, gaining increased popularity across a variety of scientific fields including social sciences, climate and environmental analysis, economics, and healthcare. Nowadays, as the accessibility of complex datasets has increased, the prevailing approach to tackling clustering challenges has transitioned from traditional algorithmic methods—such as hierarchical, partition-based, or density-based methods—to model-based methods, which assume a probabilistic modelling of the data. The Bayesian framework, in particular, offers a powerful environment for developing probabilistic models, as it allows to estimate clusters while also quantifying the uncertainty of the generated results.

Our discussion will focus on spatio-temporal clustering, which involves time series data enriched with spatial and covariates information. In particular, we will consider data on PM_{10} concentrations, collected from various measuring stations in the Lombardy region of Italy, in 2018.

A crucial aspect of spatio-temporal clustering is the ability of models to capture temporal dependencies within the sequence of partitions, allowing for a more gentle and interpretable evolution of clusters over time. Over the years, several models have been proposed in the Bayesian literature to tackle this challenge. Among them, the Dependent Random Partition Model (Page et al., 2022) stands out for explicitly addressing the temporal dependence of partitions into the model formulation. However, the current implementation of its MCMC algorithm, written in C and accessible via an R interface, lacks some significant features, which comprise the inclusion of covariates, the handling of missing data, and a more efficient implementation. The need for a more efficient implementation stems from the complexities of the spatio-temporal context, where substantial amounts of information are available and thus require scalable performance for applications on large-scale datasets.

In this work, we address these three issues by enhancing the flexibility of the original model, yielding improved performances from both the statistical and computational points of view.

2. Description of the model

The primary clustering tool employed in Bayesian clustering methods is a mixture model, where each

mixture component corresponds to a cluster with its cluster-specific parameters. In this way, each observation is assumed to arise from one of the J possible groups which are mixed together in various proportions. This formulation can be naturally extended to an infinite-mixture model, which does not necessitate a predetermined number J of components, within the framework of Bayesian nonparametrics (Grazian, 2023).

Yet, in the spatio-temporal context, where we consider a sequence of partitions evolving over time, this approach may not always be optimal. While many Bayesian nonparametric methods have been developed to temporally correlate a sequence of partitions, they typically *induce* these temporal dependencies, indirectly, resulting in weaker connections among the partitions. In contrast, the Dependent Random Partition Model (DRPM) (Page et al., 2022) explicitly models temporal dependencies among the partitions within its formulation, creating more robust temporal relationships that can be directly controlled through a dedicated parameter.

2.1. Temporal modelling for sequences of partitions

We now describe how the DRPM models temporal relationships within sequences of partitions. Before proceeding with the explanation, we first establish some general notation. We consider a spatio-temporal context where there are n units to be clustered at all time points $t = 1, \ldots, T$. Each unit is represented as $i = 1, \ldots, n$. We denote by $\rho_t = \{S_{1t}, \ldots, S_{k_t t}\}$ the partition at time t of the n experimental units, composed by k_t clusters. An alternative representation of this partition is possible through cluster labels $\boldsymbol{c}_t = \{c_{1t}, \ldots, c_{nt}\}$, with $c_{it} = j$ indicating that unit i belongs to cluster S_{jt}. Finally, we will denote with a $\star$ superscript all the variables or quantities which are cluster-specific.

Introducing temporal dependence in a sequence of partitions requires the formulation of a joint probability model for $(\rho_1, \ldots, \rho_T)$. Temporal dependence among the ρ_t's implies that the cluster configuration in ρ_t may be influenced by the cluster configurations found in $\rho_{t-1}, \rho_{t-2}, \ldots, \rho_1$. However, Page et al. (2022) restricted this temporal connection to a first-order Markovian structure, where the conditional distribution of ρ_t given all the predecessors $\rho_{t-1}, \rho_{t-2}, \ldots, \rho_1$ actually depends only on ρ_{t-1}. This led to the construction of the joint probability model for $(\rho_1, \ldots, \rho_T)$ as

$$P(\rho_1, \ldots, \rho_T) = P(\rho_T | \rho_{T-1}) \cdots$$
$$P(\rho_2 | \rho_1) P(\rho_1) \qquad (1)$$

Here, $P(\rho_1)$ is an exchangeable partition probability function (EPPF), which has the general form of $P(\rho_1) \propto \prod_{j=1}^{k_1} c(S_{j1})$ and describes how the n experimental units at time period 1 are grouped into k_1 distinct clusters a priori. For DRPM, Page et al. (2022) employed the EPPF induced by a Dirichlet process, i.e. the Chinese restaurant process, resulting in

$$P(\rho_1 | M) \propto \prod_{j=1}^{k_1} M \cdot (|S_{j1}| - 1)! \qquad (2)$$

where $|S_{j1}|$ is the cardinality of cluster S_{j1} and M is a concentration parameter that controls the number of clusters. In Section 2.2 we will detail how this EPPF can be adapted to incorporate spatial and covariates information.

To characterize the other terms $P(\rho_t | \rho_{t-1})$ in (1), the following auxiliary variables need to be introduced for all units $i = 1, \ldots, n$.

$$\gamma_{it} = \begin{cases} 1 & \text{if unit } i \text{ is } \textit{not} \text{ reallocated when} \\ & \text{moving from time } t-1 \text{ to } t \\ 0 & \text{otherwise} \end{cases}$$

These parameters model the similarity between ρ_{t-1} and ρ_t. If the partitions ρ_{t-1} and ρ_t are highly dependent, their cluster configurations will change minimally, resulting in only few units changing their cluster assignments. Conversely, partitions exhibiting low dependence will likely manifest significantly different cluster configurations, leading to a majority of the units being reallocated. By construction, we set $\gamma_{i1} = 0$ for all i, meaning that at the first time instant all units will get reallocated as there is no partition at time $t = 0$. Page et al. (2022) assumed $\gamma_{it} \overset{\text{ind}}{\sim} \text{Ber}(\alpha_t)$ where $\alpha_t \in [0, 1]$ serves as a temporal dependence parameter. Specifically, $\alpha_t = 1$ denotes perfect temporal dependence, with $\rho_t = \rho_{t-1}$, while $\alpha_t = 0$ implies full independence of ρ_t from ρ_{t-1}. For clarity, the vector $\boldsymbol{\gamma}_t = (\gamma_{1t}, \ldots, \gamma_{nt})$ is introduced, so that the T pairs of parameters $(\boldsymbol{\gamma}_j, \rho_j)$ are explicitly reported in the augmented formulation of the joint model (1), which becomes

$$P(\boldsymbol{\gamma}_1, \rho_1, \ldots, \boldsymbol{\gamma}_T, \rho_T) = P(\rho_T | \boldsymbol{\gamma}_T, \rho_{T-1}) P(\boldsymbol{\gamma}_T) \cdots$$
$$P(\rho_2 | \boldsymbol{\gamma}_2, \rho_1) P(\boldsymbol{\gamma}_2) P(\rho_1) \qquad (3)$$

Once the partition model is specified, there is considerable flexibility in how to define the remainder of the Bayesian model. The complete formulation

designed by Page et al. (2022) is provided in (4),

$$Y_{it}|Y_{it-1},\boldsymbol{\mu}_t^\star,\boldsymbol{\sigma}_t^{2\star},\boldsymbol{\eta},\boldsymbol{c}_t \overset{\text{ind}}{\sim} \mathcal{N}(\mu_{c_{it}t}^\star + \eta_{1i}Y_{it-1}, \sigma_{c_{it}t}^{2\star}(1-\eta_{1i}^2))$$

$$Y_{i1} \overset{\text{ind}}{\sim} \mathcal{N}(\mu_{c_{i1}1}^\star, \sigma_{c_{i1}1}^{2\star})$$

$$\xi_i = \text{Logit}(\tfrac{1}{2}(\eta_{1i}+1)) \overset{\text{ind}}{\sim} \text{Laplace}(a,b)$$

$$(\mu_{jt}^\star, \sigma_{jt}^\star) \overset{\text{ind}}{\sim} \mathcal{N}(\vartheta_t, \tau_t^2) \times \mathcal{U}(0, A_\sigma) \qquad (4)$$

$$\vartheta_t|\vartheta_{t-1} \overset{\text{ind}}{\sim} \mathcal{N}((1-\varphi_1)\varphi_0 + \varphi_1\vartheta_{t-1}, \lambda^2(1-\varphi_1^2))$$

$$(\vartheta_1, \tau_t) \overset{\text{iid}}{\sim} \mathcal{N}(\varphi_0, \lambda^2) \times \mathcal{U}(0, A_\tau)$$

$$(\varphi_0, \varphi_1, \lambda) \sim \mathcal{N}(m_0, s_0^2) \times \mathcal{U}(-1,1) \times \mathcal{U}(0, A_\lambda)$$

$$\{\boldsymbol{c}_t, \ldots, \boldsymbol{c}_T\} \sim \text{tRPM}(\boldsymbol{\alpha}, M) \text{ with } \alpha_t \overset{\text{iid}}{\sim} \text{Beta}(a_\alpha, b_\alpha)$$

where Y_{it} denotes the response variable measured by the i-th unit at time t and $\text{tRPM}(\boldsymbol{\alpha}, M)$ represents the temporal random partition model (3) parametrised by $\alpha_1, \ldots, \alpha_T$ and the EPPF in (2). The parameters η_{1i} and φ_1 introduce an autoregressive component at both the data level and the cluster-specific parameter level, facilitating the propagation of temporal dependence throughout the model. In particular, modelling η_{1i} through the transformation of a $\text{Laplace}(a,b)$ distribution implies less heavy tails around the boundaries of -1 and 1, thus favouring less extreme values. This choice mitigates the risk of temporal dynamics overwhelming the likelihood information, as the influence of the term $\eta_{1i}Y_{it-1}$ could cover up the contributions from the cluster-specific parameter $\mu_{c_{it}t}^\star$ and, in our updated formulation, from the regression term $\boldsymbol{x}_{it}^T\boldsymbol{\beta}_t$. Lastly, the ϑ_t parameter serves as a temporal anchor for the cluster-specific means $\mu_{jt}^\star$, ensuring that these means are not completely independent over time but instead exhibit a regular and interpretable progression.

Our generalization of the original formulation is presented in (5), with changes and additions that differ from the original model (4) highlighted in light blue.

$$Y_{it}|Y_{it-1},\boldsymbol{\mu}_t^\star,\boldsymbol{\sigma}_t^{2\star},\boldsymbol{\eta},\boldsymbol{c}_t \overset{\text{ind}}{\sim} \mathcal{N}(\mu_{c_{it}t}^\star + \eta_{1i}Y_{it-1} + \boldsymbol{x}_{it}^T\boldsymbol{\beta}_t, \sigma_{c_{it}t}^{2\star}(1-\eta_{1i}^2))$$

$$Y_{i1} \overset{\text{ind}}{\sim} \mathcal{N}(\mu_{c_{i1}1}^\star + \boldsymbol{x}_{i1}^T\boldsymbol{\beta}_1, \sigma_{c_{i1}1}^{2\star})$$

$$\boldsymbol{\beta}_t \overset{\text{ind}}{\sim} \mathcal{N}_p(\boldsymbol{b}, s^2I)$$

$$\xi_i = \text{Logit}(\tfrac{1}{2}(\eta_{1i}+1)) \overset{\text{ind}}{\sim} \text{Laplace}(a,b)$$

$$(\mu_{jt}^\star, \sigma_{jt}^{2\star}) \overset{\text{ind}}{\sim} \mathcal{N}(\vartheta_t, \tau_t^2) \times \text{invGamma}(a_\sigma, b_\sigma) \qquad (5)$$

$$\vartheta_t|\vartheta_{t-1} \overset{\text{ind}}{\sim} \mathcal{N}((1-\varphi_1)\varphi_0 + \varphi_1\vartheta_{t-1}, \lambda^2(1-\varphi_1^2))$$

$$(\vartheta_1, \tau_t^2) \overset{\text{iid}}{\sim} \mathcal{N}(\varphi_0, \lambda^2) \times \text{invGamma}(a_\tau, b_\tau)$$

$$(\varphi_0, \varphi_1, \lambda^2) \sim \mathcal{N}(m_0, s_0^2) \times \mathcal{U}(-1,1) \times \text{invGamma}(a_\lambda, b_\lambda)$$

$$\{\boldsymbol{c}_t, \ldots, \boldsymbol{c}_T\} \sim \text{tRPM}(\boldsymbol{\alpha}, M) \text{ with } \alpha_t \overset{\text{iid}}{\sim} \text{Beta}(a_\alpha, b_\alpha)$$

In our updated formulation, we model the variance parameters using an inverse gamma distribution instead of the the uniform distribution employed in (4). This more sophisticated choice should ensure better mixing in the Markov chain,

as the inverse gamma distributions recover conjugacy within the model, allowing for variance updates to be performed using the analytically exact Gibbs sampler rather than relying on the acceptance-rejection method of Metropolis algorithm. Moreover, we introduce the regression parameter $\boldsymbol{\beta}_t$, which incorporates covariates in the likelihood, with the goal of improving the accuracy in the fitted estimates of the target variable.

2.2. MCMC algorithm

We now detail the MCMC algorithm developed by Page et al. (2022), which is necessary for sampling from the posterior distributions implied by model (4). The MCMC algorithm associated to our generalized model (5) requires only minor adjustments to the original structure.

For the sake of clarity, we will refer to CDRPM for the original model formulation by (Page et al., 2022), and to JDRPM for our updated version. The letters C and J denote the programming languages used to implement their corresponding MCMC algorithms: C for the former, Julia for the latter.

The iterative structure of (3) suggests the use of a Gibbs sampler, where $\boldsymbol{\gamma}_t$ and ρ_t are updated sequentially. The Markovian assumption reduces computational costs as we only need to consider ρ_{t-1} and ρ_{t+1} when updating ρ_t. To perform this update, the terms $P(\rho_1)$ and $P(\rho_t|\rho_{t-1})$ of (3) need to be clarified. While $P(\rho_1)$ is defined by (2), the derivation of $P(\rho_t|\rho_{t-1})$ requires the concept of compatibility.

Definition 2.1 (compatibility)**.** Two partitions ρ_t and ρ_{t-1} are said to be *compatible* with respect to $\boldsymbol{\gamma}_t$ if ρ_t can be obtained from ρ_{t-1} by reallocating items as indicated by γ_t; that is, by moving the units i for which $\gamma_{it} = 0$.

To perform this compatibility check, it suffices to ensure that the reduced partitions from ρ_t and ρ_{t-1} are identical, where "reduced" refers to the restriction of partitions ρ_t and ρ_{t-1} to the units that cannot move. Indeed, if these fixed units are clustered in the same way, then the free movers from ρ_t can be assigned labels to match the ones assigned in ρ_{t-1}. Denoting the set of fixed units at time t as $\mathfrak{R}_t = \{i : \gamma_{it} = 1\}$, this check translates into verifying that $\rho_t^{\mathfrak{R}_t} = \rho_{t-1}^{\mathfrak{R}_t}$.

This compatibility must be verified during the update steps of parameters γ_{it} and cluster labels c_{it} to ensure that the new sampled draws remain valid and coherent across all partitions and parameters

involved. For instance, when updating γ_{it} during each iteration d of the algorithm, potential issues arise when transitioning from $\gamma_{it}^{(d-1)} = 0$ to $\gamma_{it}^{(d)} = 1$. This transition indicates that a unit i previously free to be reassigned (according to the parameters from the previous iteration) is now deemed to stay fixed in her cluster. However, this change may conflict with the current sampled values of partitions $\rho_{t-1}^{(d)}$ and $\rho_t^{(d-1)}$. Therefore, compatibility between their reductions to the units in the set $\mathfrak{R}_t \cup \{i\}$ needs to be checked. If this check fails, the tentative update $\gamma_{it}^{(d-1)} = 0 \rightarrow \gamma_{it}^{(d)} = 1$ is disallowed, and we enforce $\gamma_{it}^{(d)} = 0$ in the sampling algorithm.

Once this compatibility concept is introduced, we can finally derive $P(\rho_t | \rho_{t-1})$. Let $\mathcal{P}$ denote the set of all partitions of the n units and $\mathcal{P}_{C_t} = \{\rho_t \in \mathcal{P} : \rho_{t-1}^{\mathfrak{R}_t} = \rho_t^{\mathfrak{R}_t}\}$ the collection of partitions at time t that are compatible with ρ_{t-1} based on $\boldsymbol{\gamma}_t$. Then, by construction, we find that $P(\rho_t | \rho_{t-1})$ is a random partition distribution with support $\mathcal{P}_{C_t}$ and density

$$P(\rho_t = \lambda | \boldsymbol{\gamma}_t, \rho_{t-1}) = \frac{P(\rho_t = \lambda)\mathbb{1}_{[\lambda \in \mathcal{P}_{C_t}]}}{\sum_{\lambda'} P(\rho_t = \lambda')\mathbb{1}_{[\lambda' \in \mathcal{P}_{C_t}]}}$$

While this formulation is not statistically appealing, Page et al. (2022) proved that, under the construction outlined thus far, marginally $\rho_1, \ldots, \rho_T$ are identically distributed with law derived from the EPPF used to model ρ_1. This result, along with the previously outlined compatibility analysis, enables the derivation of the complete update rules rules for γ_{it} and c_{it}.

Once the sampling scheme for γ_{it} and ρ_t is established, updating the other parameters of the model becomes straightforward. Each parameter will be updated using its full conditional distribution. For most parameters, this distribution is available due to the conjugacy of their associated priors in the model, while for a few others a Metropolis step is required. The complete derivation of the full conditional distributions is straightforward and is extensively detailed in the thesis. The update rule for the missing Y_{it} values involved sampling from its full conditional distribution, which was derived using computations similar to those for the model parameters.

We will now outline the final theoretical step, which addresses how spatial and covariates information can be incorporated into the prior for the partitions.

The core of the clustering process, that is, updat-

ing γ_{it} and ρ_t, is inherently complex as it necessitates checking for compatibility issues. The approach entails simulating the assignment of each unit i, currently belonging to cluster j, to either one of the existing clusters or to a new singleton cluster. For each scenario, we compute the probability of this assignment to occur, from which we derive weights to inform the sampling decision for the next iteration. To influence the definition of these weights by spatial and, in our JDRPM updated formulation, covariates information, the EPPF (2) has to be updated through dedicated cohesion and similarity functions, respectively.

2.3. Spatial cohesions

The incorporation of spatial information can be effectively accommodated through the EPPF in our framework, resulting in spatially informed clusters that evolve over time. To introduce this extension, let $\boldsymbol{s}_i$ denote the spatial coordinates of the i-th (we note that these coordinates do not change over time), and let $\boldsymbol{s}_{jt}^\star$ denote the subset of spatial coordinates of the units belonging to cluster S_{jt}. Then, we can express the EPPF for the t-th partition in the following product form

$$P(\rho_t | M, \mathcal{S}) \propto \prod_{j=1}^{k_t} C(S_{jt}, \boldsymbol{s}_{jt}^\star | M, \mathcal{S}) \qquad (6)$$

Compared to the original formulation of (2), where $P(\rho_t | M) \propto \prod_{j=1}^{k_t} c(S_{jt} | M)$, (6) incorporates a spatial component into the partition weights through the spatial cohesion function $C(S_{jt}, \boldsymbol{s}_{jt}^\star | M, \mathcal{S})$. The original term $c(S_{jt} | M)$ describes how units inside cluster S_{jt} are likely to be clustered together a priori, while the cohesion function $C(S_{jt}, \boldsymbol{s}_{jt}^\star | M, \mathcal{S})$, parametrised by a set of parameters $\mathcal{S}$, measures the compactness of the spatial coordinates $\boldsymbol{s}_{jt}^\star$. In the JDRPM code, we implement the same six cohesion functions which were also implemented in CDRPM, specifically, those described in (Page et al., 2016).

2.4. Covariates similarities

The incorporation of covariates information, a characteristic feature of our generalized model, can be similarly integrated into the EPPF definition. To introduce this extension, let $X_{jt}^\star$ denote the $p \times |S_{jt}|$ matrix that contains the p covariates of the units belonging to cluster S_{jt}, i.e. $X_{jt}^\star = \{\boldsymbol{x}_{it}^\star = (x_{it1}, \ldots, x_{itp})^T : i \in S_{jt}\}$. In the current implementation of JDRPM we decided to treat each covariate individually. In this way, the

new term in the definition of the EPPF for $P(\rho_t)$ will be a function of the vector $\boldsymbol{x}^\star_{jtr}$ that collects the values of the r-th covariate for the units inside cluster S_{jt}, i.e. row r of matrix $X^\star_{jt}$. Then, each contribution of the covariates will be considered independently, leading to an EPPF in the form

$$P(\rho_t|M,\mathcal{S},\mathcal{C}) \propto \prod_{j=1}^{k_t} C(S_{jt}, \boldsymbol{s}^\star_{jt}|M,\mathcal{S}) \left(\prod_{r=1}^{p} g(S_{jt}, \boldsymbol{x}^\star_{jtr}|\mathcal{C}) \right) \quad (7)$$

Here, $g(S_{jt}, \boldsymbol{x}^\star_{jtr}|\mathcal{C})$ is the covariate similarity, parametrised by a set of parameters $\mathcal{C}$, which measures the similarity of the covariates values $\boldsymbol{x}^\star_{jtr}$. This approach of treating each covariate individually is convenient as it simplifies the definition of the similarity functions and allows to accommodate both numerical and categorical covariates. In the JDRPM code, we implement four similarity functions, which are detailed in (Page et al., 2018).

3. Implementation

To implement the MCMC algorithm to compute the posterior samples of our generalized model, described in Section 2.2, we chose the Julia language (Bezanson et al., 2017).

Julia is a relatively new programming language that combines the ease and expressiveness of high-level languages with the efficiency and performance of low-level languages. This balance is primarily achieved through just-in-time compilation, using the LLVM framework, along with features as dynamic multiple dispatch and extensive code specialization against multiple run-time types.

As we will discuss in Section 4.2, we obtained improved performance in Julia, compared to the original C implementation of (Page et al., 2022), despite the increased complexity of the model and the associated MCMC algorithm. This performance gain was largely possible through various refinements and optimizations which we now briefly outline.

In fact, during the earlier development phases, we observed that a substantial portion of execution time was not spent by actual calculations, but rather by Julia's garbage collector, which had the burden of tracking all the allocated memory and reclaiming the unused one to make it available for new computations. To address this issue, we refactored the code to operate more in-place. This approach involved passing as arguments the variables that would be modified by a function, and applying those changes directly within the

function, rather than returning values and subsequently using them to update the original variables. This optimization strategy was facilitated by Julia profiling tools such as `ProfileCanvas` and `BenchmarkTools`.

Another relevant performance improvement was achieved through the optimized implementation of spatial cohesions and covariates similarities. In fact, these functions are essential for deriving the partition weights in the update steps of γ_{it} and ρ_t, and as such they are potentially executed millions of times during each fit. Therefore, refining these functions was crucial for providing fast execution times. In the cohesions functions, optimal performance was reached by using static vectors and matrices, provided by the `StaticArrays` package, rather than standard dynamic structures. For the similarity functions, we employed a SIMD paradigm (Single Instruction Multiple Data), through the `@simd` macro, which accelerated the elaboration of the covariates values by working on multiple data-chunks at once, rather than processing each element individually.

4. Analysis of the models

To evaluate the numerical performance of both algorithms, we analysed posterior samples and clusters estimates in two scenarios: first using a synthetic dataset that includes only the response variable, and secondly employing a real-world spatio-temporal dataset. For the latter, we used a dataset from the AgrImOnIA project (Fassò et al., 2023) which encompasses weekly measurements of air pollutants in 2018, together with many other environmental variables, in the Lombardy region of Italy. This dataset also provides covariates, whose effects will be examined in Sections 4.1.1 and 4.1.2.

4.1. Statistical improvements

In the first set of experiments we fitted the two models, in both simulated and real-world scenarios, under equivalent conditions—i.e. identical datasets, hyperparameters, and MCMC configurations. With this setup, the models are expected to perform similarly to each other, as JDRPM is a generalization of CDRPM and should therefore manifest the same core behaviour of the original model. Indeed, the clusters estimates, as well as their temporal trend depicted in Figures 1 and 2, were remarkably similar, thus confirming the correctness of the JDRPM implementation. Moreover, the fitted values were more ac-

curate in the JDRPM fits, as demonstrated by the mean squared errors (MSEs) improved by 20% and 8% in the simulated and real-world scenarios, respectively, compared to CDRPM fits. In absence of additional information from covariates, this improvement was likely attributable to the better mixing properties of the Markov chain in our model, thanks to the distribution choice for the variance parameters.
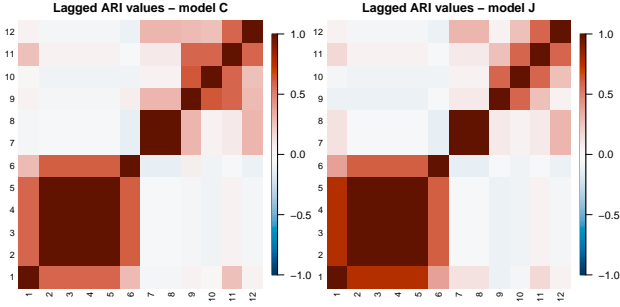

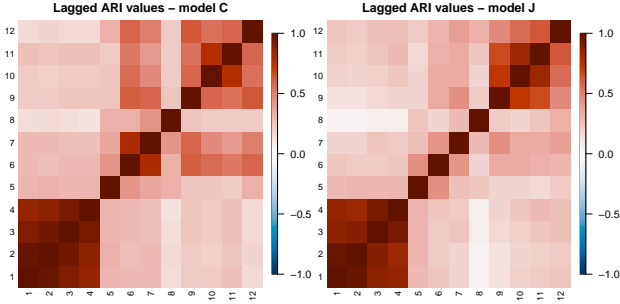Figure 1: Lagged ARI values of CDRPM and JDRPM fits, in the simulated data scenario.

Figure 2: Lagged ARI values of CDRPM and JDRPM fits, in the real-world scenario.

Next, we investigated the effects of covariates-informed fits. Given their different roles, we studied separately covariates in the likelihood and covariates in the prior.

4.1.1 Covariates in the likelihood

The inclusion of covariates in the likelihood through the regression term $\boldsymbol{\beta}_t$ had the main goal of improving the accuracy of the fitted values. Therefore, we examined two natural use-cases of covariates in the likelihood: first, fitting on spatio-temporal dataset with missing data, and second, performing inference on a new unit at a new location.

In the first experiment, we performed JDRPM fits on an incomplete dataset, generated by randomly removing 10% of the data points from the full dataset. Indeed, the inclusion of covariates in the likelihood from the spatio-temporal dataset

resulted in improvements across all metrics, as proved by the reduced MSEs and better LPML and WAIC. The results are presented in Table 1.

Table 1: Comparison of JDRPM fits, in the real-world scenario, with and without the inclusion of covariates in the likelihood, on a complete dataset and on a dataset with missing values.

	Full data	Full data + Xlk	NA data	NA data + Xlk
MSE (mean)	0.0131	**0.0112**	0.0160	**0.0127**
MSE (median)	0.0138	**0.0113**	0.0170	**0.0130**
LPML	624.91	**778.96**	502.86	**625.81**
WAIC	-1898.05	**-2029.84**	-1793.64	**-1902.74**
Execution time	**48m**	56m	**43m**	58m

We also mention that the standard fits without covariates in the likelihood did not exhibit a significant drop in performance, compared to their full dataset counterparts. This indicates that even in the absence of additional information, the update rule for the missing data Y_{it} remains effective. For example, in the simulated scenario with missing data, where covariates information was not available, all the true values of the missing points fell within the 95% credible intervals of the corresponding fitted estimates, as reported in Figure 3.
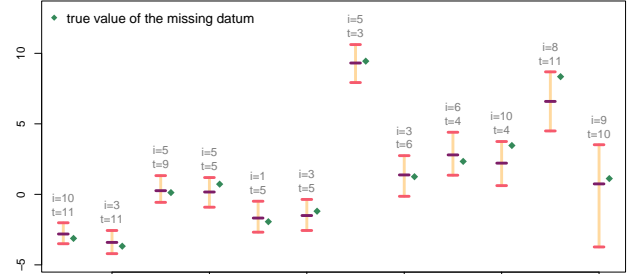

Figure 3: Credible intervals, computed with the highest posterior density method at a 95% confidence, for the fitted values of the missing units in the JDRPM fit, in the simulated data scenario, on a dataset with missing values. In gray are reported the indexes of units i and time instants t which where set to missing values, while green dots refer to the true values of those missing data points.

In the second experiment, we simulated the insertion of new units at new locations by removing all data entries from three randomly selected units within the spatio-temporal dataset. In this way, we aimed to evaluate the JDRPM's accuracy in predicting the behaviour of units for which sensors may be absent or inactive, and we expected that the estimation accuracy would improve as model complexity increases. Indeed, the best performances, in terms of MSE, LPML, and WAIC, was achieved by JDRPM fits with covariates in the likelihood; proving again the effectiveness of

this addition to the model formulation. Figures 4 and 5 display the 95% credible intervals of the estimated target values for the missing units, derived from the two JDRPM fits with only spatial information and with also covariates in the likelihood.

Notably, some inaccuracies were observed in the case of the red unit. This particular unit was often clustered as a singleton, exhibited extreme values in some of the included covariates, and was quite separate from other units. Thus, these particular factors possibly hindered a more precise estimation of her response variable values.
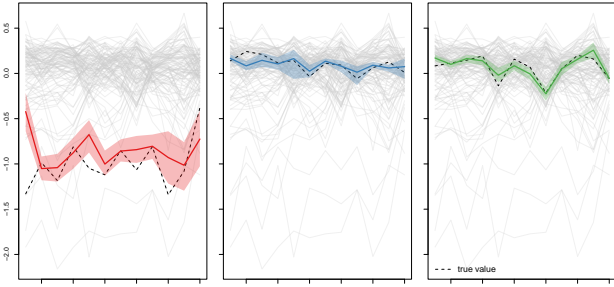
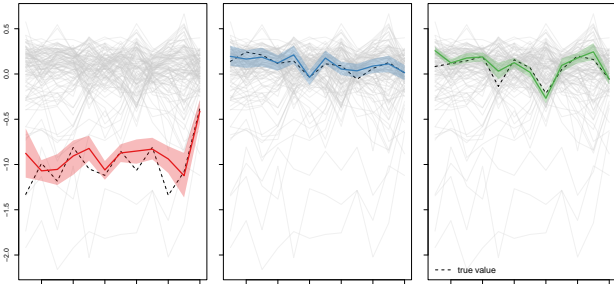Figure 4: Inference analysis of JDRPM on new locations, in the spatially-informed fit.

Figure 5: Inference analysis of JDRPM on new locations, in the spatially-informed fit with covariates in the likelihood.

4.1.2   Covariates in the prior

The main goal of incorporating covariates in the prior was to generate more informative and accurate clusters configurations. Therefore, in this set of experiments, we performed several JDRPM fits on the PM_{10} target variable, but now including three relevant covariates in the prior: wind speed and precipitation levels (Liu et al., 2020), along with boundary layer height (Huang et al., 2021). The boundary layer height measures the maximum height at which air mixing occurs, with lower values indicating a higher expected concentration of pollutants due to restricted vertical mixing. In fact, as air rises in the atmosphere, it typically cools. However, there are instances where warm air exists above colder air, which can inhibit

air mixing. In such cases, pollution accumulates without a means of dispersal, resulting in a deterioration of air quality.

Again, the inclusion of covariates information displayed a significant improvement across all metrics, as reported in Table 2.

Table 2: Comparison between CDRPM and JDRPM fits and their associated algorithms, in the real-world scenario, with and without covariates in the prior.

	CDRPM	JDRPM	JDRPM + Xcl
MSE (mean)	0.0142	0.0131	**0.0126**
MSE (median)	0.0149	0.0138	**0.0135**
LPML	694.81	624.91	**677.71**
WAIC	-1768.42	-1898.05	**-1969.76**
Execution time	1h38m	**48m**	1h20m

The inclusion of multiple covariates in the prior can often lead to a greater number of smaller, more specific clusters. This is due to the additional information available to the model, which enhances its ability to identify dissimilarities between units. This effect can be illustrated through cluster-specific boxplots of the target variable PM_{10} alongside the three covariates included in the analysis.

As shown in Figure 6, the spatially and covariates-informed JDRPM fit captured a more refined and coherent clustering structure, demonstrating a clear separation in both the target variable PM_{10} and the covariates, particularly regarding wind speed and total precipitation. This increased specialization of clusters allows for clearer interpretation of the results. For instance, cluster 2 is characterized by the highest levels of PM_{10} and the second-last levels of wind speed and total precipitations, suggesting that these environmental factors likely hindered pollutant dispersion, making this cluster the most polluted. Another example can be seen in clusters 3 and 4, which exhibit similar PM_{10} levels but completely different precipitation levels, demonstrating the model's capability to capture finer distinctions between the clusters. The contribution of covariates is particularly evident when comparing the CDRPM spatially-informed fit to the JDRPM fit including space and covariates in the prior. Such comparison, exemplified by Figures 7 and 8, demonstrates how the JDRPM fit was more effective in identifying clusters that appeared, instead, sparser and less specialized in the CDRPM fit.
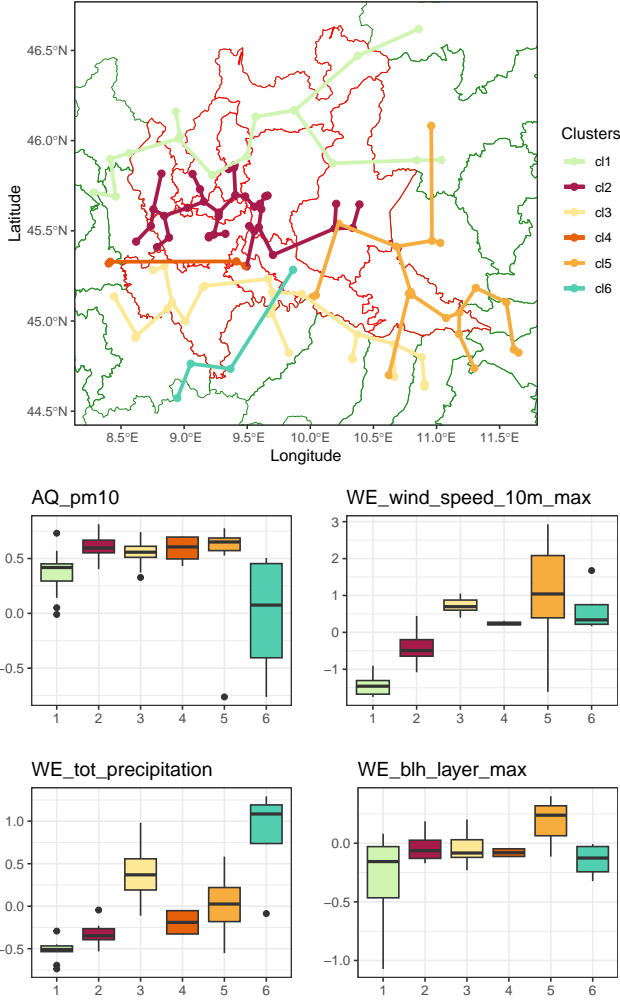
Figure 6: Example of the clusters estimates produced by JDRPM fit, in the real-world scenario, with covariates in the prior. The boxplots refer to the target variable `AQ_pm10` along with the three covariates included in the fit.

4.2. Computational improvements

Finally, to rigorously assess whether the objective of faster execution times was achieved, we designed a series of experiments to compare the two models and their corresponding implementations. The varying levels of information influence model complexity, which in turn affects computational load; however, also the size of the testing dataset also plays a significant role. To systematically investigate these factors, we conducted experiments across incremental levels of information—starting with only the target variable, then adding spatial information, covariates in the likelihood, and finally covariates in the prior—as well as across a "mesh" of dataset sizes, with both the number of units n and the time horizons T ranging through the set $\{10, 50, 100, 250\}$. It is important to note that results from datasets with extreme sizes, such as those with n or T being 250, may reflect hardware limitations of the machine used for fitting,
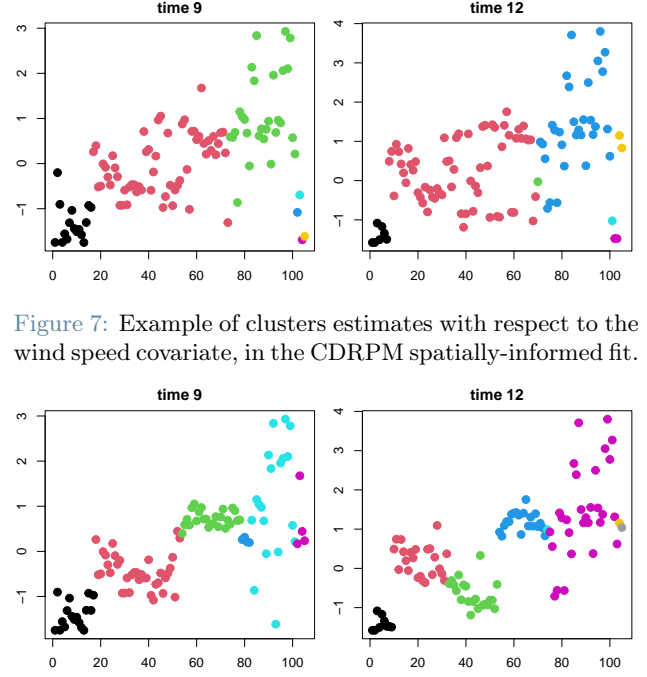

Figure 7: Example of clusters estimates with respect to the wind speed covariate, in the CDRPM spatially-informed fit.

Figure 8: Example of clusters estimates with respect to the wind speed covariate, in the JDRPM spatially-informed fit with covariates in the prior.

i.e. my simple laptop, rather than actual model performance. Therefore, more attention should be devoted to the more accurate intermediate-sized experiments, which firmly demonstrate the JDRPM's improved performance. For instance, Figure 9 proves that, in the case of spatially-informed fits, JDRPM can operate up to twice as fast as CDRPM.

Figure 9: Execution times, in milliseconds per iteration, when fitting JDRPM on a spatio-temporal dataset. In brackets are reported the speedups relative to the CDRPM timings, where higher values indicate better performance.

Moreover, JDRPM fits including covariates infor-

mation still exhibit strong performance, despite the additional complexity and subsequent increase in computational load. Figure 10 illustrates that, on a medium sized dataset consisting of $n = 50$ units, fully-informed JDRPM fits can perform faster than spatially-informed CDRPM fits. In addition, we can observe how JDRPM fits with spatial information can perform faster than CDRPM fits without spatial information.

In Figure 10, the number of covariates in the likelihood and prior levels was fixed to $p = 5$. This configuration appears to represent the equilibrium point between JDRPM and CDRPM performances. More precisely, other experiments were conducted with varying numbers of covariates in likelihood and prior levels, demonstrating how in the same amount of time that CDRPM performs a spatially-informed fit, JDRPM can perform a spatially-informed fit with up to five covariates in the prior and with an almost indifferent number of covariates in the likelihood, as covariates in the likelihood do not add significant computational load. These results strongly support the performance speedup achieved with our new implementation.
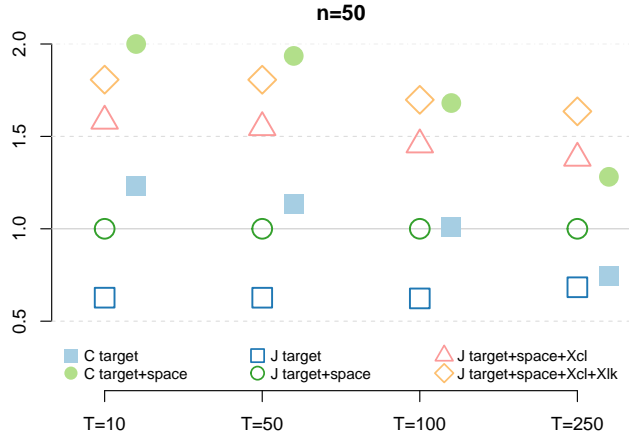

Figure 10: Visual representation of the performance of all the fits, for the $n = 50$ case. Specifically, the execution time per iteration of JDRPM spatially-informed fit has been taken as a reference, to which then all other fits have been compared to derive their speedup (or slowdown) factor. Points above the reference line indicate slower fits, while points below denote faster fits.

5. Conclusions

In conclusion, we can state that JDRPM represents a significant improvement over the original formulation of CDRPM. From a theoretical perspective, JDRPM retains the foundational structure of its predecessor, while also introducing covariates in the prior and likelihood levels, as well

as providing more flexibility through the handling of missing data in the target variable. From a computational perspective, we successfully reduced execution times compared to the original implementation of Page et al. (2022). Moreover, the innovative choice of the Julia language is expected to facilitate the implementation of future modifications or updates.

However, potential drawbacks arise from the increased complexity of our generalized model. The choice of a more sophisticated distribution for the variance parameters, along with the selection of parameters for spatial cohesions and covariates similarities, may necessitate more careful consideration and experimental tuning when performing a model fit. To this end, future development paths could focus on mitigating this complexity, e.g. through heuristics for assigning the various parameters and hyperparameters given the dataset at hand. Additionally, the Julia powerful ecosystem could be leveraged to provide real-time feedbacks on the sampling process, e.g. through live trace plots of the sampled values or logs detailing the progression of MCMC update steps.

In summary, while the JDRPM's complexity may present certain challenges, it also establishes a foundation for significant methodological advancements and practical enhancements. Our developments are expected to improve the model's applicability and accuracy, ultimately leading to more effective research outcomes.

References

Bezanson, Jeff et al. (2017). "Julia: A fresh approach to numerical computing". In: *SIAM Review* 59.1, pp. 65–98. DOI: 10.1137/141000671 (cit. on p. 5).

Fassò, A. et al. (2023). *AgrImOnIA: Open Access dataset correlating livestock and air quality in the Lombardy region, Italy (3.0.0)*. DOI: https://doi.org/10.5281/zenodo.7956006 (cit. on p. 5).

Grazian, Clara (Mar. 2023). "A review on Bayesian model-based clustering". In: DOI: 10.48550/arXiv.2303.17182 (cit. on p. 2).

Huang, Yaxuan et al. (2021). "Relative importance of meteorological variables on air quality and role of boundary layer height". In: *Atmospheric Environment* 267, p. 118737. ISSN: 1352-2310. DOI: https://doi.org/10.1016/j.atmosenv.2021.118737. URL: https://www.sciencedirect.com/science/article/pii/S1352231021005598 (cit. on p. 7).

Liu, Zhen et al. (2020). "Analysis of the Influence of Precipitation and Wind on PM2.5 and PM10 in the Atmosphere". In: *Advances in Meteorology* 2020.1, p. 5039613. DOI: `https://doi.org/10.1155/2020/5039613` (cit. on p. 7).

Page, Garritt L. and Fernando A. Quintana (Sept. 2018). "Calibrating covariate informed product partition models". In: *Statistics and Computing* 28, pp. 1–23. DOI: `10.1007/s11222-017-9777-z` (cit. on p. 5).

– (2016). "Spatial Product Partition Models". In: *Bayesian Analysis* 11.1, pp. 265–298. DOI: `10.1214/15-BA971` (cit. on p. 4).

Page, Garritt L., Fernando A. Quintana, and David B. Dahl (2022). "Dependent Modeling of Temporal Sequences of Random Partitions". In: *Journal of Computational and Graphical Statistics* 31.2, pp. 614–627. DOI: `10.1080/10618600.2021.1987255` (cit. on pp. 1–5, 9).